Efficient Methanol Dehydration to DME and Light Hydrocarbons by submicrometric ZrO_2-ZSM-5 fibrillar catalysts with a shell-like structure.

José Palomo, Miguel A. Rodríguez-Cano, José Berruezo-García, José Rodríguez-Mirasol* and Tomás Cordero

Universidad de Málaga, Andalucía Tech, Departamento de Ingeniería Química, 29010 Málaga, Spain.

ABSTRACT

Zeolites are widely used in many applications, such as catalysis and adsorption processes. The use of these materials in a nanometric size would be of great interest for these applications, due to the better performance they could exhibit in terms of avoiding intraparticle mass and heat transfer limitations. However, this small particle size results in high pressure drops in adsorption columns and fixed-bed reactors, making these materials non-applicable directly in the nanometric size. In this work, ZrO_2 fibers with a mean diameter of 275 nm and the presence of small well-defined ZSM-5 zeolite aggregates of 550 nm in size around the ZrO_2 submicrometric fibers, in the form of a shell-like structure, have been prepared by electrospinning technique, which resulted very active for the synthesis of DME and light olefins via methanol dehydration. The submicrometric fibrillar catalysts, without any further modification, could be easily structured inside a fixed-bed reactor, which worked very efficiently in terms of heat and mass transfer, avoiding, at the same time, the usual pressure

drops problems of fixed-bed reactors working with catalyst particles of submicrometric size. Methanol conversion and selectivity to DME and light hydrocarbons could be finely controlled, for a given set reaction conditions, by tuning the zeolite loading in the structured catalyst. Apparent kinetic parameters for the selective methanol dehydration to DME were calculated assuming a reversible second order rate expression and an activation energy of 75 kJ/ mol was obtained.

Keywords: Core-shell, dimethyl ether, electrospinning, zeolite, fibers, nanostructured catalysts.

*corresponding author: Prof. Dr. José Rodríguez-Mirasol, e-mail address: *mirasol@uma.es*, Phone number: (+34) 951952385.

1.- Introduction

Zeolites, an important kind of crystalline aluminosilicates, are widely used in many applications, such as, carbon dioxide capturing [1], catalysis [2] and gas sensing [3]. These materials present a network of channels at a molecular scale, which provides these aluminosilicates a uniform and ordered microporous structure [4]. This well-defined microporosity confers the materials a high surface area, along with an excellent stability and unique shape selectivity.

Most of the current zeolites are used in a particulate form or structure according to their applications [5,6]. These materials are usually commercialized in

powder form, with particle sizes ranging from several thousands of nanometers to several microns [7]. This small particle size favors the intraparticle mass transfer of the reactants and products. However, it also results in high pressure drops in fixed-bed reactors, making these materials non-applicable directly. To overcome this issue, zeolites need to be mixed with other compounds in order to be pelletized or even structured in form of monolith. This packing process usually results in the decrease of the specific surface area [8,9] and, thus, in the loss of efficiency of the material [10,11]. Therefore, although pressure drops limitations could be overcome by different strategies, the loss of performance derived from these agglomeration processes is still a pending issue that need to be addressed.

Besides, the microporous size of the channels present in the structure of the zeolite is frequently translated into intraparticle diffusion limitations [4,12], especially in catalysis applications. Moreover, highly exothermic reactions could also introduce heat transfer problems [13], giving rise to hotspots in chemical reactors that may seriously damage the catalyst. Regarding these issues, there is a growing interest in directly using nanosized zeolites [14–17], due to the improvement of mass transfer of the reactant to the active sites.

One of the applications for zeolite materials that is receiving a great deal of attention is their use as acid catalyst for methanol dehydration to selectively produce dimethyl ether (DME) [18,19] or light olefins [20,21]. DME is a chemically stable, non-toxic and environmentally friendly compound. Due to its physical and chemical properties, similar to those of liquified petroleum gases (LPG) [22] and conventional diesel [23,24], plus the clean combustion achieved when used as fuel [25], this compound is considered as one of the most

promising alternatives to petroleum derived fuel and, thus, the study of DME production has been the object of intensive research [26–28]. Currently, methanol dehydration on an acid catalyst is the main process to produce DME. Selective methanol dehydration to DME has been widely investigated using several solid acid catalyst [6,14,29]. Among them, zeolites have been intensively investigated, due to the excellent catalytic performance they present. On this issue, Rownaghi et al. [14] reported that scaling down the zeolite crystal size to the nanometric scale resulted in the enhancement of the catalytic activity and selectivity to DME, as compared to conventional zeolite particle sizes, due to the higher number of pore entrances available for reactant and products for the nanosized zeolite. Catizzone et al. [18] also observed that the use of submicron-sized zeolite crystals led to an increase of the apparent methanol turn over frequency (TOF) due to the improved mass transfer in the process and to the enhanced accessibility to the active sites, when compared with conventional sized zeolites. On the other hand, the use of zeolites as catalysts for methanol dehydration to light olefins (Methanol to Olefins -MTO- process), is also receiving much attention. MTO process is nowadays considered as a valuable alternative synthetic route to fulfil the increasing worldwide demand of ethylene and propylene [30]. In order to attain a high yield towards light olefins, a low zeolite crystal size has been reported to be beneficial [31]. On this issue, some authors reported the preparation of zeolite-supported catalysts, which allow the feasible operation of a fixed-bed reactor, in terms of pressure drops, while keeping a short reaction path for light olefins, preventing their further conversion to higher hydrocarbons. Ivanova et al. [32], reported the preparation of ZSM-5/-βSiC foam structured catalysts, which overperformed conventional

zeolite catalysts beds, in terms of activity and selectivity to light olefins, for the MTO process. Zhang et al. [33] prepared ZSM-5 zeolite supported catalysts via hydrothermal synthesis on perlite supports, which demonstrated a fairly good catalytic activity for the light olefins production by MTO. However, the preparation of these catalyst is not straightforward, making necessary complex experimental methodologies that involve several stages. Therefore, the establishment of new synthesis approaches for the ease preparation of zeolite supported catalysts still remains a challenge.

Electrospinning is a simple and straightforward technique that has been used to obtain carbonaceous and polymeric fibers in the submicron and nanoscale [34,35]. In this process, a viscous polymer solution, held by its surface tension at the end of a capillary tube, is subjected to a high voltage electric field, inducing the ejection of a charged liquid jet to a collector electrode. Due to the electrostatic repulsions between the surface charges, an unstable whipping of the jet occurs in the space between the capillary tip and the collector electrodes, provoking the solvent evaporation and leading to the deposition of polymeric fibers on the collector [36]. This technique has been proved to be a very efficient approach for the preparation of catalysts [34,37,38]. On the preparation of zeolite fibers, a few studies can be found in the literature. Anis and Hashaikeh [39] reported the preparation of electrospun zeolite-Y fibers. Liu et al. [37] reported the preparation of hollow ZSM-5 fibers and the application of this material into the iso-butane catalytic cracking. These experimental procedures lead to the preparation of continuous zeolite fibers. However, highly exothermic reactions, such as MTO, could introduce heat transfer problems in chemical reactors, giving rise to the formation of un-anticipated hotspots that may

seriously damage the catalyst. Under this high exothermic scenario, catalyst particles need to be diluted in the fixed-bed to avoid such hotspots generation inside the reactor [13,40] and, thus, the application of the reported fibrillar materials could be restricted.

In this study, we report a straightforward method for the one-step preparation of submicrometric structured zirconia-zeolite fibrillar materials by using the electrospinning technique. By this way, ZSM-5 zeolite submicron particle aggregates covering the zirconia fibers in a shell-like structure, homogeneously separated (diluted), along the zirconia fiber have been prepared. We also report the use of these materials as efficient catalysts for methanol dehydration to dimethyl ether and light olefins.

2.- Experimental method

2.1.- Preparation of fibrillar catalysts

The experimental procedure followed for the preparation of the fibers presented in this work involves the preparation of a polymer solution, the electrospinning of the resulting solution and the calcination of the prepared fibers.

Zirconium acetate solution was used as zirconia precursor and PVP was added to obtain the polymeric solution, giving the suitable viscosity to make the solution electrospinnable. The Zirconium-PVP solution was prepared by mixing 5 g of zirconium acetate solution diluted in acetic acid (Sigma–Aldrich, CAS 7585-20-8, $Zr^{+x}{\cdot}xCH_3COOH$, Zr ~16 % (w/w)) and 350 mg of polyvinylpyrrolidone, PVP (CAS 9003-39-8, Mw = 1,300,000). The resulted

145 solution was vigorously stirred for 12 h up to transparency. The addition of
146 different amounts of ZSM-5 (MFI) zeolite (Zeolyst international, CBV 5524G,
147 SiO_2/Al_2O_3 50, with mean crystal size of 120 nm) and 1 g of acetic acid to this
148 zirconium-PVP solution resulted in the preparation of different zeolite-zirconium-
149 PVP suspensions, which were vigorously stirred for 10 hours. The
150 concentrations of zeolite in the polymeric solutions were adjusted to obtain
151 zeolite contents ranging from 5 to 50 %(w/w) in the final fiber, after calcination.
152 The electrospinning set-up used for the electrospun process consisted of a
153 syringe pump, a needle or spinneret, a plate collector and two high voltage
154 power suppliers. In a typical experiment, the flow rate of the solution through the
155 spinneret was set to 0.5 mL/h, the tip-to-collector distance was 20 cm and the
156 electrical potential difference was 14 kV. Samples prepared following this
157 procedure were denoted as FZrXZ, where X refers to the zeolite loading mass
158 percentage.

159 Finally, the as-spun fibers were recovered in form of non-woven cloth and then
160 calcined in a muffle furnace at 500 ºC for 4 h under air atmosphere, to eliminate
161 the remaining solvent, the polymer and any carbon deposit, stabilize the
162 zirconia fibers and to transform the zeolite from the ammonium to the hydrogen
163 form.

164 *2.2.- Characterization of the catalytic materials.*

165 The surface morphology of the samples was studied by scanning electron
166 microscopy (SEM) using a Jeol JSM-6490LV microscope working at 20 kV
167 voltage and by transmission electron microscopy (TEM) in a FEI Talos F200X
168 microscope at an accelerating voltage of 200 kV and in a high annular dark field
169 (HAADF). Three dimensional (3D)-TEM measurements were carried out using a

FEI Talos F200X microscope at 200 kV and in a high annular dark field (HAADF), where 2D-projections images with tilt angles ranging from -70 to 70º (206 TEM images in total) were automatically acquired. 3D images were reconstructed using Amira-Avizo for FEI and Inspect3D software.

The porous texture of the prepared fibers was characterized by N_2 adsorption-desorption at -196 ºC and by CO_2 adsorption at 0 ºC, carried out in an ASAP 2020 equipment (Micromeritics). Samples were previously outgassed for 8 h at 150 ºC under vacuum. From the N_2 isotherm, the apparent surface area (A_{BET}) was determined by applying the BET equation [41]; the application of t method using Harkins and Jura equation allowed the estimation of the micropore volume (V_t) and the external surface area (A_t) [42]; mesopore volume (V_{mes}) was calculated as the difference between the maximum adsorbed volume of N_2 (V_p), at a relative pressure of 0.95 and the micropore volume (V_t). From CO_2 adsorption data, the narrow micropore surface area (A_{DR}) and the narrow micropore volume (V_{DR}) were assessed using the Dubinin-Radushkevich equation [43].

X-ray diffraction patterns (XRD) of the calcined fibers were recorded in the region 2θ= 5-90 º on an EMPYREAN PANalytical diffractometer using CuKα monochromatic radiation (operation value 45 kV and 40 mA), using a PIXcel detector and Soller slits (incident and diffracted beam) of 0.04 rad. The average size of the crystal phases was calculated by applying the Williamson-Hall method [44].

The acid strength distribution and total acidity of the prepared fibers were determined by temperature programmed desorption of ammonia (NH_3-TPD). For NH_3-TPD analyses, 100 mg of the prepared material was firstly heated up

to 500 ºC at a heating rate of 10 ºC/min, and then cooled to 100 ºC under helium flow. Then the sample was saturated with NH_3 (20 % (v/v) in helium) for 15 minutes at 100 ºC. After saturation, the weakly adsorbed NH_3 was desorbed in helium flow at the same temperature, until no NH_3 was detected in the outlet stream. The NH_3-TPD was carried out rising the temperature up to 500 ºC at a heating rate of 10 ºC/min under continuous helium flow. The outlet NH_3 concentration was registered using a TCD-detector.

2.2.- Catalytic experiments.

Gas phase methanol dehydration experiments were carried out at atmospheric pressure in a fixed-bed microreactor (i.d. 4 mm) placed inside a vertical furnace with temperature control. In a typical experiment, 150 mg of fibers were used. Methanol was fed to the system by using a syringe pump (Cole-Parmer® 74900-00-05 model), using helium as carrier gas, which ensured a constant controlled methanol flow. The reaction was carried out in the temperature range of 180-450 ºC. To avoid condensation of any compound, all lines were heated up to 120 ºC. The feed conditions used were a methanol partial pressure of 0.10 atm ($1.013 \cdot 10^4$ Pa) and at different space times 0.002 - 0.01 ($g_{ZSM\text{-}5} \cdot s/\mu mol_{MeOH}$). The conversion was defined as the ratio of the amount of methanol converted to the amount of methanol supplied to the reactor and was expressed in molar %. The selectivity (in %mol) was defined as the ratio of carbon moles in a specific product divided by moles of converted methanol. The apparent turnover frequency (TOF) values were calculated as the moles of methanol converted per hour and per acid site, at a reaction temperature of 180 ºC.

The outlet gas concentrations were quantified by on-line gas chromatography (Perkin-Elmer Clarus 500 GC equipped with TCD and FID detectors). The

columns used were a Permanent gases active carbon 80/100 mesh for CO, CO_2 analysis, and a 1.9m x 1/8” x 2.1mm Porapak N 80/100 + 0.5m x 1/8” x 2.1mm Porapak Q 80/100 column for methanol, DME and light hydrocarbons separation. N_2 was used as internal standard for GC analyses.

3.- Results and discussion

3.1.- Zirconia-Zeolite fibers characterization

The morphology of the zirconia-zeolite fibers was examined by scanning electron microscopy (SEM) and transmission electron microscopy (TEM). Fig. 1a presents a SEM image of the prepared zirconia fibers. The size and shape of these fibers was highly uniform, with diameters ranging from 200 to 300 nm. Moreover, it could be observed the absence of fused zones or beads. Fig. 1b shows a SEM image of the zirconia-zeolite fibers with a 10 %(w/w) of ZSM-5 zeolite. In this case, two well-defined structures could be appreciated. The material was mainly composed by smooth fibers, similar to the zirconia fibers observed in Fig. 1a, and small well-defined particle aggregations along the fibers, presenting an average size of about 550 nm, homogeneously spaced (diluted) along the fiber.

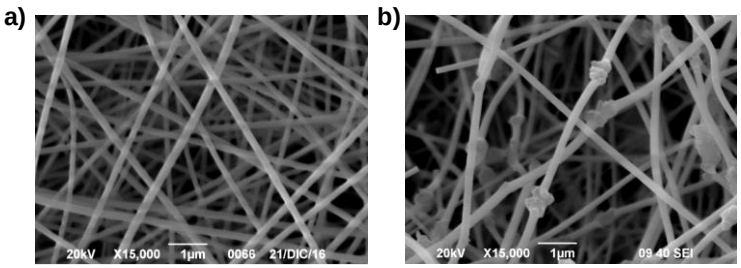

Fig. 1. Scanning electron micrographs of the fibers calcined at 500 ºC in air (a) zirconia fibers, (b) zirconia-zeolite fibers (10 % (w/w) zeolite).

The chemical composition of the two different phases presented on the zirconia-zeolite fibrillar materials was analyzed by transmission electron microscopy energy-dispersive X-ray spectroscopy (TEM-EDXA). Fig. 2a shows a high-angle annular dark field scanning transmission electron microscopy (HAADF-STEM) image along with the Zr and Si EDXA elemental mappings composite of a region of the material containing a particles aggregation. As expected, the smooth fibrillar part of the material was only composed by zirconium oxide, since no Si was detected in this region. In contrast, the particles aggregation region exhibited the presence of both Zr and Si, evidencing the presence of aggregates of zeolite particles, in a similar way to the ones reported for SiO_2 [45] and polystyrene nanoparticles [46]. A reduction of the particle size has been reported to cause the formation of aggregates into clusters of particles around the fibers, due to the smaller particles have relatively large surface energy and the diameter of the fiber is larger than the size of particles, so the particles have to pack together [45]. Fig 2b shows 3D-TEM/electron tomography images from various rotation angles of a region of the fiber containing a zeolite particles aggregation. From these 3D images it can be observed that the zeolite particles assembling seemed to occur, in this case, surrounding the zirconium oxide submicron fiber, creating local shell-like structures with sizes ranging from 350 to 550 nm. The average size of the zeolite particles in the aggregates obtained from TEM analyses showed a value of 120 nm. X-ray diffraction (XRD) analyses of the zeolite containing samples further confirmed the presence of the two crystalline phases, zeolite (ZSM-5) and tetragonal zirconium oxide (see Fig.

S1). From XRD analyses, the mean crystal size value of these zeolite particles was estimated as 60 nm, by applying the Williamson-Hall method.

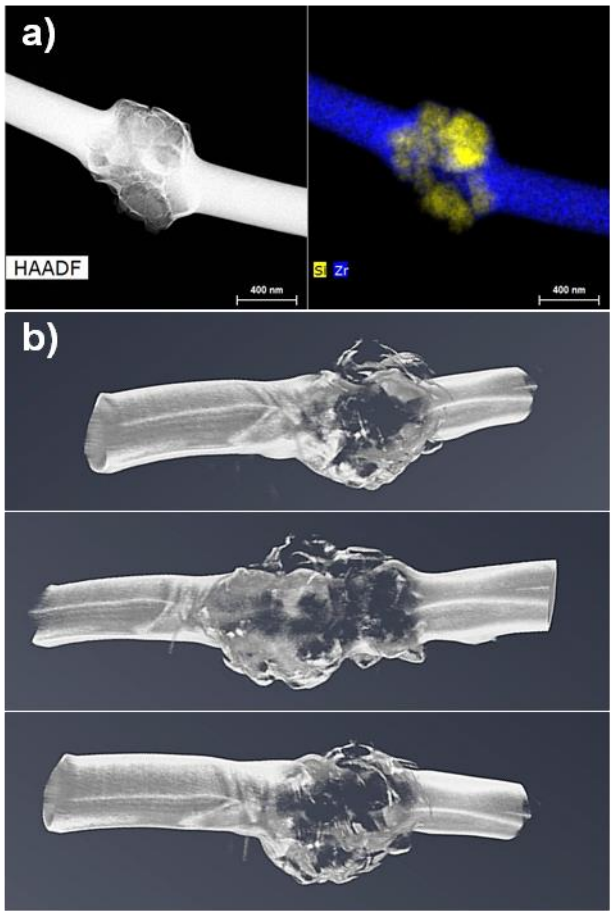

Fig. 2. a) HAADF-STEM image, and Si (yellow) and Zr (blue) EDXA elemental mappings composite, of a zeolite particles aggregation in the zirconia-zeolite fibers. Scale bar is 400 nm. b) 3D-TEM/electron tomography images from various rotation angles of a region of the fiber containing a zeolite particles aggregation.

The increase of the zeolite concentration in the electrospinning solution resulted in a higher proportion of the local zirconia-zeolite aggregates in the form of shell-like structures, with the corresponding reduction of the distance between these zirconia-zeolite shell-like structures along the fibers (see Fig. 3). The

average measured distance for the separation between the zeolite aggregates showed values of 9.5, 4.5 and 1.75 μm, for zeolite concentrations of 5, 10 and 15 %(w/w), respectively. Thus, a linear relationship between the zeolite content and the distance separating the local zeolite aggregates in the form of core-shell like structures along the fibers was observed, in this loading range. When the zirconium fibers containing a zeolite content of 20 %(w/w) were analyzed, the distance between the zeolite aggregates along the fiber continued to decrease, showing an average value of 0.91 μm. Moreover, it was observed that the zirconia-zeolite shell-like structures started to join for zeolite loadings higher than 20 %(w/w). Actually, for the case of the sample containing a 50 %(w/w) of zeolite a hybrid fibrillar material with ZSM-5 zeolites covering the zirconia fibers as in a shell-like structure was observed (Fig. 3b).

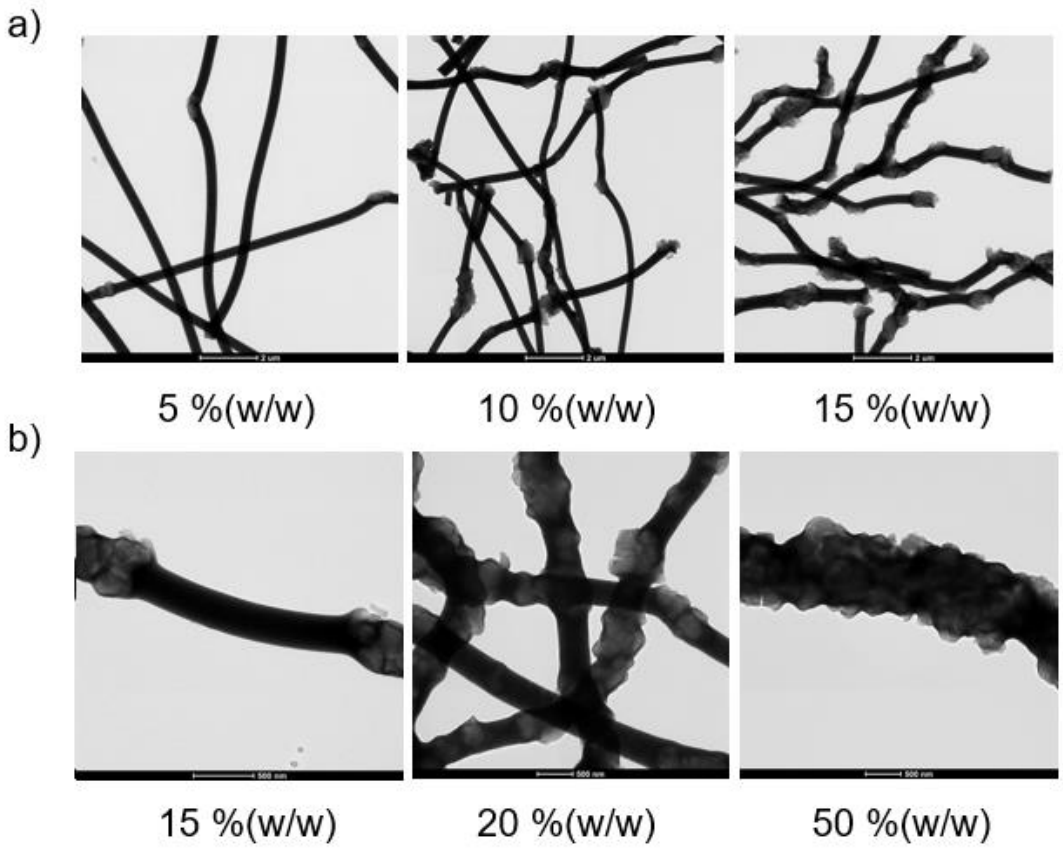

Fig. 3. Transmission electron micrographs for the zirconia-zeolite fibers. Effect of % (w/w) zeolite in the final fiber. a) Scale bar is 2 μm. b) Scale bar is 500 nm.

N_2 adsorption-desorption studies were carried out in order to evaluate the possible loss of textural properties in the zeolite as a consequence of the preparation process. Fig. 4a presents the N_2 adsorption-desorption isotherms at -196 ºC for the ZSM-5 zeolite along with the zirconia and the zirconia-zeolite fibrillar materials prepared in this study. Zirconia fibers, FZr, showed very low N_2 adsorption, suggesting a non-porous texture. ZSM-5 zeolite showed a type Ib isotherm, which is characteristic of solids with narrow microporosity [47]. N_2 uptake of the zirconia-zeolite fibers showed a high dependence on the zeolite content, especially in the range of low relative pressures. In this sense, the higher the zeolite content, the higher the N_2 adsorption. H4 hysteresis loop was observed for the zeolite and zirconia-zeolite fibers, which is associated to zeolite nanocrystal aggregations [47]. CO_2 adsorption isotherms showed the same trend, indicating that the presence of the narrow microporosity is mainly related to the presence of zeolite in the fibrillar materials (Fig. 4b).

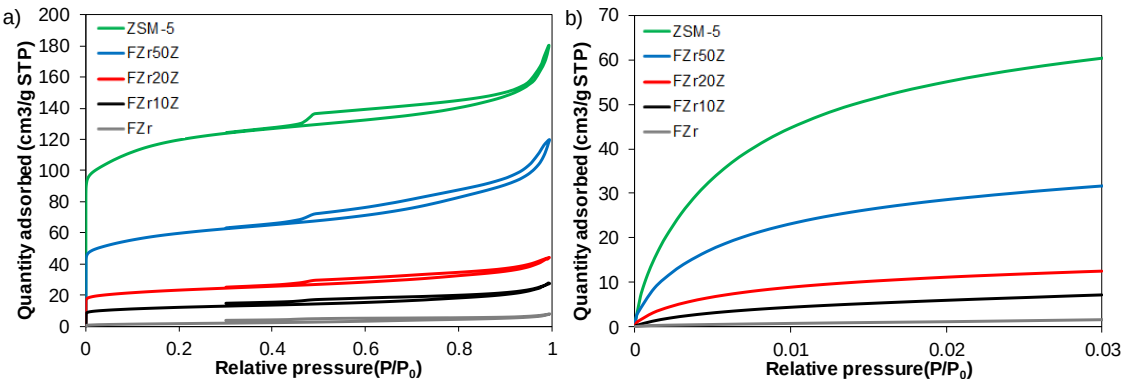

Fig. 4. a) N_2 adsorption–desorption isotherms at −196 ºC and b) CO_2 adsorption at 0 ºC of ZSM-5 zeolite, the zirconia and the zirconia zeolite fibers.

Table 1 summarizes the characteristic parameters derived from the N_2 adsorption-desorption and the CO_2 adsorption isotherms. The calculated Bruneauer-Emmett-Teller (BET) specific surface area (A_{BET}) for the powder zeolite, ZSM-5, and the zirconia fibers, FZr, showed values of 442 and 7 m^2/g, respectively. When analyzing the zirconia-zeolite fibers, it was found that the value of this parameter increased with the zeolite content of the sample, showing values close to the proportional sum of the pure zeolite and the zirconia fibers. In this sense, the calculated values for the fibers containing a 10, 20 and 50 %(w/w) of zeolite, were 42, 82 and 217 m^2/g, respectively. A_{DR} values calculated from CO_2 adsorption isotherms showed the same trend, further suggesting that the microporous texture of the raw zeolite is not deteriorated during the preparation of the structured catalysts. However, this trend was not observed when analyzing the external surface area, A_t^{N2}, which showed higher values than the predicted by the proportional sum of their individual components in all prepared fibrillar materials. In this sense, the A_t^{N2} values normalized to the zeolite content showed the following figures: 1.5, 1.2, 1.1 and 0.5 m2/g for the fibers containing a 10, 20 and a 50 % of zeolite loading and the raw zeolite, respectively, which suggest that the more isolated the zeolite nanoparticles are, the higher external surface area. Therefore, the preparation procedure here presented did not caused a loss of accessibility to the zeolite internal surface in the hybrid fibrillar material. Furthermore, the final hybrid fibrillar material presented a high external surface area, which is very relevant for catalysis applications.

Table 1. ZSM-5 loading, characteristic parameters of the porous texture, and acidity determined by NH_3-TPD of the different catalysts.

	% ZSM-5 %(w/w)	A_{BET}^{N2} (m^2/g)	V_p^{N2} (cm^3/g)	A_t^{N2} (m^2/g)	V_t^{N2} (cm^3/g)	A_{DR}^{CO2} (m^2/g)	V_{DR}^{CO2} (cm^3/g)	Acidity (μmol NH_3/g)
FZr	0	7	0.01	7	0	4	0	31
FZr10Z	10	42	0.04	15	0.01	53	0.02	181
FZr20Z	20	82	0.07	24	0.03	95	0.04	280
FZr50Z	50	217	0.19	56	0.07	229	0.09	585
ZSM-5	100	442	0.28	51	0.17	509	0.20	977

Acid properties of the materials here presented were studied by temperature programmed desorption of ammonia (NH_3-TPD). Table 1 contains the total amount of ammonia desorbed during TPD, obtained by the integration of the area under NH_3-TPD curves. Zirconia fibers, FZr, desorbed a negligible amount of ammonia during NH_3-TPD analysis, which indicated the low acidic character of this material. As it occurred with the textural parameters, the total acidity of the zirconia-zeolite materials linearly increased with the amount of ZSM-5, indicating that the acidity of these materials could be mainly attributed to the presence of zeolite. Fig. 5 presents the NH_3-TPD profiles obtained for the parent ZSM-5 zeolite along with the prepared zirconia and the zirconia-zeolite fibers. ZSM-5 zeolite showed two ammonia desorption peaks, with maximum at 225 and at 410 ºC, respectively. The former could be associated to weak acid sites, probably of Lewis nature, while the latter could be related to ammonia interacting with strong Bronsted acid sites present on the surface of the zeolite material [48]. The ammonia desorption profiles obtained for the zirconia-zeolite fibers showed the same shape that the one of the ZSM-5 zeolite, being the main difference the intensity of the ammonia desorption peaks, associated to the zeolite content in the fibrillar material. Hence, it can be concluded that the

acid sites of the parent zeolite and their acid strength distribution remained unaltered when preparing the fibrillar materials.

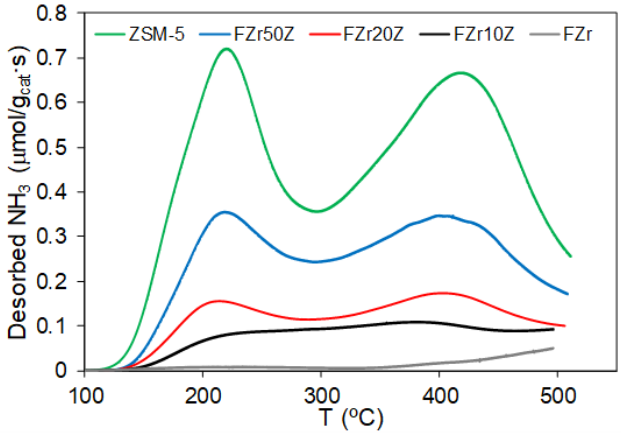

Fig. 5. Ammonia TPD profiles of the ZSM-5 zeolite along with the zirconia and the zirconia-zeolite fibers.

3.2. Catalytic dehydration of methanol on the fibrillar catalysts

3.2.1. Calculation of the internal and external mass and heat transfer related parameters.

Methanol dehydration experiments were carried out in a fixed bed microreactor (i.d. 4mm) using the fibrillar materials here presented as catalysts, in the temperature range 180 – 450 ºC. The homogeneous phase reaction contribution was found to be negligible for temperatures below 600 ºC. Axial dispersion problems were not considered given that a value of L_b/d_p (being L_b the bed length and d_p the particle diameter) was calculated to be $4 \cdot 10^4$ for the experimental conditions used in the present study [49,50].

The absence of external and internal mass-transfer limitations was theoretically assessed. External mass transfer limitations were evaluated by using the

Carberry number (Ca) [51]. A value of $1.73 \cdot 10^{-8}$ was calculated for the Ca number under the experimental conditions used in this study, which is well below 0.05. Therefore, effect of external mass-transfer limitations can be considered negligible. The isothermal intraphase internal effectiveness factor, η, which is a function of the Thiele modulus, ϕ, was used for the evaluation of the internal mass-transfer limitations. The calculated values for the Thiele modulus and the internal effectiveness factor were, $5.3 \cdot 10^{-3}$ and 1, respectively, which clearly highlight the absence of internal mass-transfer limitations.

The absence of extraparticle and intraparticle heat transfer limitation phenomena was also theoretically assessed following the criteria stated by Moulijn et al. [51]. According to these criteria, for the consideration of negligible external and internal heat transfer limitations, the system must satisfy $\gamma \cdot \beta_e \cdot Ca < 0.05$ and: $\gamma \cdot \beta_i \cdot (\eta \cdot \varphi 2) < 0.1$, respectively.

$$\gamma \cdot \beta_e \cdot Ca = \left(\frac{E_a}{R \cdot T_b}\right) \cdot \left|\frac{(-\Delta H_r) \cdot k_f \cdot c_b}{h \cdot T_b}\right| \cdot \left(\frac{r_{v,obs}}{a' \cdot k_f \cdot c_b}\right) = 5.71 \cdot 10^{-8} < 0.05 \qquad \text{(Eq. 1)}$$

$$\gamma \cdot \beta_i \cdot (\eta \cdot \phi^2) = \left(\frac{E_a}{R \cdot T_b}\right) \cdot \left|\frac{(-\Delta H_r) \cdot D_{eff} \cdot c_s}{\lambda_{eff,p} \cdot T_b}\right| \cdot \left(\frac{r_{v,obs} \cdot L^2}{D_{eff} \cdot c_s}\right) = 1.7 \cdot 10^{-9} < 0.1 \quad \text{(Eq. 2)}$$

In the equations stated above, $\gamma = E_a/R \cdot T$, is the Arrhenius number, $\beta_{e,i}$ is the external or internal temperature gradient and $(\eta \cdot \varphi^2)$ is the Wheeler-Weisz modulus. The calculated values for the parameters required by both criteria clearly fulfill the conditions for neglecting the effect of external and internal diffuse limitations in the present study.

3.2.2. Selective methanol dehydration to DME

391 The zirconia-zeolite fibrillar materials here presented were directly used as
392 catalyst bed for the methanol dehydration reaction, without any further
393 modification. Fig. 6 shows the steady-state methanol conversion as a function
394 of the ZSM-5 loading for the fiber-based catalysts at a reaction temperature of
395 250 ºC (P_{MeOH} = 0.10 atm, W/F_{MeOH} = 0.02 g_{CAT}·s/μmol_{MeOH}). Zirconia fibers, FZr,
396 not containing zeolite, showed a negligible catalytic activity for this reaction at
397 these conditions, due to the low acidity this material presented. As expected,
398 methanol conversion increased with ZSM-5 content in the zirconia-zeolite fibers,
399 since the surface acidity and, thus, the catalytic activity was related to the
400 presence of this phase in the material. A very high selectivity to DME (100 %)
401 was observed for all the materials studied at these operating conditions.

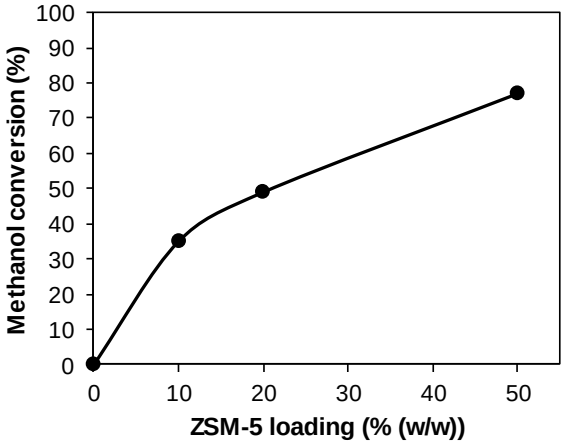

402

403 Fig. 6. Methanol conversion as a function of Zeolite loading for zirconia-zeolite
404 fibers at a constant temperature of 250 ºC (P_{MeOH}=0.10 atm (1.013 ·10^4 Pa),
405 W/F_{MeOH}=0.02 g_{CAT}·s/μmol_{MeOH}).

406 Zeolite materials have been widely investigated for the selective dehydration of
407 methanol to DME [6,14,29]. Rownaghi et al. [14] studied the effect of the zeolite
408 crystal size in methanol conversion and selectivity to DME. In their study, they

observed that scaling down the zeolite crystal size to the nanometric size resulted in a higher methanol conversion. This fact was attributed to the higher number of pore entrances available on the nanocrystal surface, as compared to the one of the conventional zeolite particle size [14]. More recently, Catizzone et al. [6] reported an increase of the apparent turn over frequency (TOF) when reducing the zeolite crystal size to the submicrometric size, which was ascribed to the improved mass transfer in the process and to the enhanced accessibility to the active sites. However, it is worth to mention that for the application of nanocrystal zeolitic materials in a fixed-bed reactor, they must be pelletized in order to avoid high pressure drops. On the contrary, the fibrillar catalysts reported in the present work, showing submicrometric sizes, were synthetized through a simple one-step process and were (after calcination) directly used in a fixed-bed reactor. The load of the fibrillar nanostructured catalyst in the fixed-bed reactor resulted in the formation of a structured catalyst bed, which performed very efficient in terms of intraparticle mass and heat transfer (see Section 3.2.1), avoiding, at the same time, the problems related to pressure drops of fixed-bed reactors working with such a reduced particle size. On this issue, the pressure drop value inside the reactor was also theoretically calculated and compared to the value obtained for a catalyst bed conformed by powder catalyst particles with the same effective dimension. The fibrillar catalytic bed analyzed in the present work (average radius of the fibers= 250 nm) showed a porosity value of 0.97, which is very high as compared to the values usually found for particle packed beds (ranging from 0.35 to 0.47) [52], and is in good agreement with the porosity values reported by Jackson and James for different fibrillar materials [53]. For the operation conditions used in

434 this study, the Reynolds number for porous media (Re_{mp}) showed a value of
435 $1.73 \cdot 10^{-4}$, indicating a laminar flow regime, in which the pressure drop value can
436 be estimated by combining the Darcy's Law along with the Kozeny-Carman
437 equation [54]. The pressure drops for this fibrillar packed bed showed a value of
438 0.59 bar/m. On the other hand, the pressure drop value calculated for a packed
439 bed reactor containing spherical particles presenting the same dimensions as
440 those of the fibers (average radius of the particles= 250 nm), was 6500 bar/m,
441 which is several orders of magnitude higher than the value calculated for the
442 fibrillar packed bed. These theoretical results further back-up the advantage of
443 using fibrillar catalyst in fixed-bed reactors.

444 The fibrillar catalysts here presented performed very efficient for the selective
445 methanol dehydration to DME, in terms of methanol conversion and selectivity
446 to DME, with no deactivation with time on stream observed at the reaction
447 conditions studied (see Fig. S2a). This stability with time on stream also
448 indicated that no zeolite dropped during reaction. Table 2 shows a compilation
449 of methanol dehydration to DME catalytic activities for different catalysts
450 reported in the literature. As can be observed, higher conversion values than
451 those reported for non-zeolite catalyst, such as activated carbon-based [55],
452 mesoporous silica [56] and alumina-based [57,58] catalyst, were achieved,
453 even working in the present work at much higher space velocity. As compared
454 to other zeolite materials, the fibrillar catalysts here presented also
455 outperformed other zeolite catalysts [14,59]. On the other hand, higher
456 conversion values than the ones achieved in the present study can be found in
457 the literature when using ferrierite as catalyst [60]. However, it should be noted
458 that the space velocity used in those studies is around 3 times lower than the

459 one used in here (4 vs 11,5 h^{-1}). In this sense, the apparent turnover frequency
460 (TOF), calculated at 180 ºC for the fibrillar catalysts here used, showed a value
461 of 52 h^{-1}, which is within the range of apparent TOF values reported by
462 Catizzone et al. [6] (45 – 65 h^{-1}) for ferrierite catalysts. These results clearly
463 highlight the good catalytic performance of the submicron fibrillar catalysts here
464 presented.

465 Table 2. Summary of the catalytic results obtained for selective methanol
466 dehydration to DME on different catalysts.

Catalyst	T (ºC)	X_{CH3OH} (%)	S_{DME} (%)	WHSV (h^{-1})	Reference
FZr10Z	300	70	100	57.7[a]	This work
FZr50Z	225	53	100	11.5[a]	This work
FZr50Z	250	72	100	11.5[a]	This work
γ-χ-Al_2O_3	250	41	100	1.3[b]	[57]
Fe_2O_3/γ-χ-Al_2O_3	250	46	100	1.3	[58]
Nano-ZSM-5	225	44	100	2.6	[14]
Al-MCM-41	250	35	99	1.3[b]	[56]
N-FER	240	85	99	4	[60]
ACPZr	300	30	97	14.7[c]	[55]
Zeolite W	300	20	100	2	[59]

[a] Calculated with respect to the ZSM-5 content (active phase) in the catalyst bed

[b] Calculated from the stated experimental conditions (methanol flow and catalyst mass)

[c] Calculated from the stated experimental conditions (methanol flow and active phase content in the catalyst bed).

467

468 Apparent kinetic parameters for the selective methanol dehydration to DME
469 were estimated from conversion vs temperature profiles, obtained at different
470 zeolite loadings in the catalyst bed (space-times), and considering that

methanol dehydration reaction (Eq. 3) kinetics can be described by a reversible second order rate expression (Eq. 4).

$$2\,CH_3OH \quad \rightleftharpoons \quad CH_3OCH_3 \quad + \quad H_2O \quad \text{(Eq. 3)}$$

$$r_{DME} = k \cdot \left(P_{CH3OH}^2 - \frac{P_{CH3OCH3} \cdot P_{H2O}}{K_{eq}} \right) \quad \text{(Eq. 4)}$$

In Eq. 4, k is the apparent rate constant ($mol_{MeOH} \cdot g_{ZSM\text{-}5}^{-1} \cdot s^{-1} \cdot atm^{-1}$), which follows an Arrhenius type dependence with temperature; P_{CH3OH}, $P_{CH3OCH3}$ and P_{H2O} represents the methanol, DME and water vapor partial pressures, respectively; and K_{eq} is the equilibrium constant for the methanol dehydration reaction, which can be described as a function of the temperature as follows (Eq. 5) [61]:

$$\ln\left(K_{eq}\right) = \frac{2835.2}{T} + 1.675 \cdot \ln(T) - 2.39 \cdot 10^{-4} - 0.21 \cdot 10^{-6} \cdot T^2 - 13.360 \quad \text{(Eq. 5)}$$

Further assuming a uniform distribution of the active sites in the catalyst bed, steady-state operation and negligible heat and mass transfer limitations (see Section 3.2.1), a plug flow integral reactor was considered for the interpretation of the experimental data. For this purpose, the reactor mass balance equation (Eq. 6) was numerically integrated to calculate the methanol conversion at the reactor outlet.

$$P_{M,0} \frac{dx_M}{d\left(\frac{W_{ZSM-5}}{F_{M,0}}\right)} = (-r_M) = 2 \cdot r_{DME} \quad \text{(Eq. 6)}$$

In the above expression, $W_{ZSM\text{-}5}$ is the weight of zeolite in the catalyst bed, $F_{M,0}$ is the methanol molar flow rate fed to the reactor and x_M is the methanol conversion.

The calculation of the kinetic parameters, preexponential factor and activation energy, was carried out by minimizing the quadratic difference between the experimental and the simulated methanol conversion values. Fig. 7 shows the simulated and the experimental methanol conversion values as a function of the temperature for different space times. As can be observed, this kinetic model is capable of reproducing the experimental data with a very high accuracy. The calculated preexponential factor and activation energy values were $3.9 \cdot 10^4$ $mol_{MeOH} \cdot g_{ZSM\text{-}5}^{-1} \cdot s^{-1} \cdot atm^{-1}$ and 75 kJ/mol, respectively. The value of activation energy calculated in the present work is in good agreement with other studies available in the literature, dealing with methanol dehydration to DME using zeolite catalysts, which reported values for this kinetic parameter ranging from 52- 61 kJ/mol [40,62,63] to 90-100 kJ/mol [64–66].

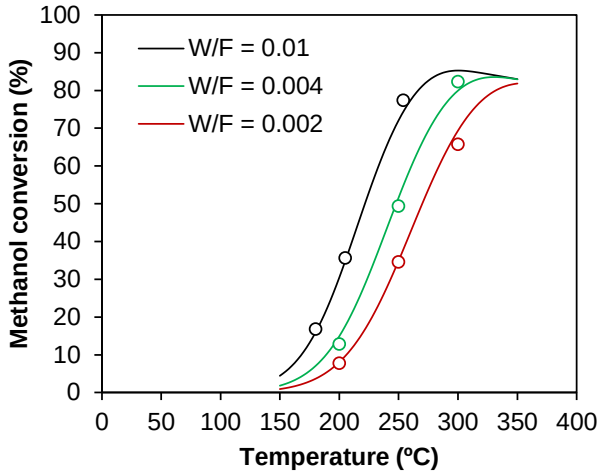

Fig. 7. Simulated (solid lines) and experimental (open dots) steady-state methanol conversion as a function of the reaction temperature for the fibrillar catalysts at a constant partial pressure of methanol P_M=0.1 atm ($1.013 \cdot 10^4$ Pa), for different $W_{ZSM\text{-}5}/F_{M,0}$ (space time).

3.2.3. Methanol dehydration to olefins

510 The presence of acid sites with a high strength on the surface of ZSM-5 zeolite,
511 further promotes DME dehydration to hydrocarbons [67,68]. In order to attain a
512 high yield towards low olefins, the use of a low zeolite crystal size has been
513 claimed to be beneficial [31]. Aiming to allow a feasible operation of a fixed bed
514 reactor, in terms of pressure drops, when using a very low zeolite particle and
515 crystal size, the use of supported zeolite catalysts has been explored
516 [32,33,69,70]. However, the preparation methodologies required for the
517 synthesis of these structured catalysts involve several complex and costly
518 stages. Conversely, as already stated, the preparation methodology here
519 reported allows a simple and straightforward synthesis of structured fibrillar
520 catalysts. Furthermore, it is also interesting to mention that by the experimental
521 methodology here presented it is also feasible to obtain a uniform and
522 controlled acid sites density on the catalysts (through the separation -or dilution-
523 of the core shell-like nanostructures, in the submicrometric scale), by simply
524 adjusting the amount of ZSM-5 zeolite in the electrospinning solution.

525 The effect of space time (in terms of zeolite content in the catalyst bed) and
526 reactor temperature over the product distribution was also analyzed in the
527 present study. Zirconia fibers, FZr, not containing zeolite, showed a methanol
528 conversion lower than 5% up to 400 ºC, yielding DME as a major product, which
529 is in agreement with the low acidity this material present. Fig. 8a and b show the
530 evolution of the methanol conversion and selectivity to the main products as a
531 function of reaction temperature, respectively, for a fibrillar catalyst containing a
532 20 %(w/w) zeolite. An increase in the reaction temperature resulted in a higher
533 methanol conversion. Regarding the selectivity to the main reaction products,
534 the high selectivity (100%) to DME in the temperature range of 200-300 ºC was

remarkable. At higher temperatures (350-400 ºC), the selectivity to light hydrocarbons (C2- C4) was also outstanding (higher than 60 %), which makes these materials also very attractive for the methanol to olefins (MTO) process [33,71]. Regarding the stability of the catalyst, no deactivation was observed, at least, up to 10 hours of time on stream (at 400 ºC) (see Fig. S2b). After this time, the catalyst just experienced a partial deactivation, presumably due to coke deposition [72,73] on the strongest acid sites and, afterwards, it continued keeping a total functionality for the selective methanol dehydration to DME, with no further deactivation.

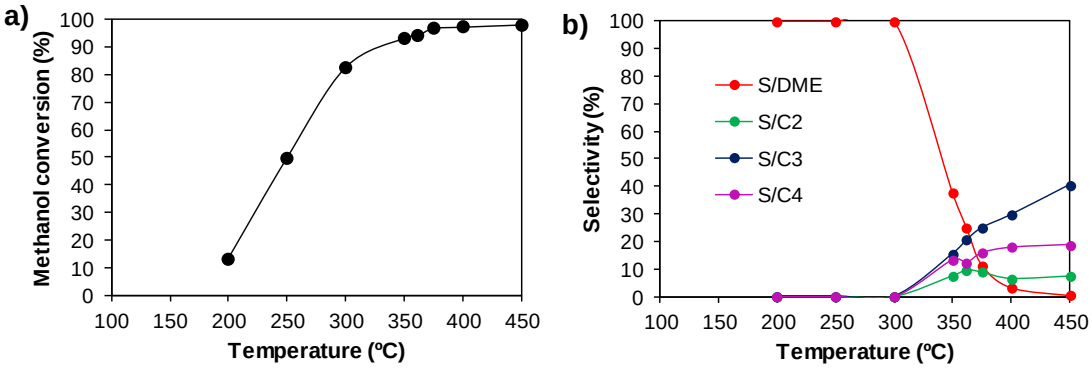

Fig. 8. a) Methanol conversion and b) selectivity to DME and light olefins as a function of the temperature for the catalyst containing a 20 %(w/w) zeolite (P_{MeOH}=0.10 atm, W/F_{MeOH}=0.004 $g_{ZSM\text{-}5}$·s/μmol_{MeOH}).

The selectivity towards DME and light hydrocarbons at different temperatures for a constant bed mass of the zirconia-zeolite fibrillar catalysts, with zeolite loadings of 10, 20 and 50 %(w/w), are summarized in Table 3. DME was further converted to light olefins when rising the temperature. The temperature value at which selectivity to DME dropped was related to the zeolite content in the catalyst (or the space time with respect to the zeolite mass in the reactor).

Among the light olefin products, selectivity to C2 and C3 increased with the amount of zeolite in the catalyst, for similar reaction temperature and methanol conversion values. In this sense, the increase of methanol conversion and selectivity to light hydrocarbons could be finely controlled by increasing the zeolite loading in the catalyst, for other set reaction conditions.

It is also worth to mention that high exothermic reactions, such as MTO process, could introduce heat transfer problems in chemical reactors, giving rise to the formation of unexpected hotspots that may seriously damage the catalyst bed, particularly, in the presence of water vapor for zeolites. In order to avoid such scenario, conventional catalyst size particles need to be diluted in the fixed-bed reactor to avoid this hotspots generation inside the reactor [13,40]. As an alternative to conventional particulate catalysts, the preparation methodology here reported yields structured fibrillar catalysts with a tunable separation between submicron nanostructured zeolite aggregates along the fiber, which could act as a diluted bed, once inside the reactor. By this way, it is possible to set the separation distance between the active catalyst nanoparticles (dilution) within the catalyst bed, which could be beneficial for the control of heat accumulation processes inside the reactor, while keeping a high mass transfer due to the reduced active phase particle size, and, thus, for a more efficient reactor operation. Furthermore, it is also interesting to point out that, once packed in a fixed bed reactor, very high (and tunable) void fractions could be obtained (up to 0.95), while using immobilized particles, which could be also an interesting feature when using chemical reactors working at a larger scale.

579 Table 3. Methanol conversion and selectivity to DME and light hydrocarbons, at
580 different temperatures, for the zirconia-zeolite fibrillar catalysts with zeolite
581 loadings of 10, 20 and 50 %(w/w), (P_{MeOH} = 0.10 atm, W/F_{MeOH} = 0.02
582 $g_{cat}·s/\mu mol_{MeOH}$).

Catalyst	Temperature	X_{MeOH}	S_{DME}	S_{C2}	S_{C3}	S_{C4}
FZR10Z	300	65.8	100	0	0	0
	350	84.48	100	0	0	0
	375	87.9	48.5	3.0	15.7	7.7
	400	92.7	20.1	3.3	29.0	14.9
FZR20Z	300	82.4	100	0	0	0
	350	93.2	37.5	7.6	15.5	13.4
	375	96.5	11.4	8.9	24.9	15.9
	400	97.1	3.19	6.6	29.7	17.9
FZR50Z	300	90.2	63.7	8.0	9.4	2.8
	350	93.5	1.7	12.0	20.7	15.0
	375	97.7	0.4	9.6	27.0	19.0
	400	98.1	0.1	8.9	32.9	20.9

583

584 ## 4.- Conclusions

585 Electrospinning is a useful technique for the one-step preparation of submicron
586 (nanostructured) ZrO_2-ZSM-5 fibrillar materials in the form of core-shell like
587 structures. SEM and TEM images showed fibers with a high aspect ratio and
588 mean sizes of 275 nm and the presence of zeolite aggregates around the ZrO_2
589 nanofiber, in the form of core-shell like structures. X-ray diffraction (XRD)
590 analyses further confirmed the presence of both zirconia and ZSM-5 zeolite

591 crystal phases. The submicron nanostructured fibrillar catalysts here presented
592 could be easily packed inside a fixed-bed reactor, without any further
593 modification, and worked very efficiently for the methanol dehydration reaction
594 in terms of heat and mass transfer, avoiding, at the same time, the usual
595 pressure drops problems of fixed-bed reactors working with catalyst particles of
596 submicrometric size.

597 The experimental methodology here presented allowed to the feasible obtention
598 of a uniform and controlled acid sites density (dilution) in the catalyst bed
599 through the separation of the core shell-like nanostructures, in the
600 submicrometric scale, by simply adjusting the amount of ZSM-5 zeolite in the
601 electrospinning solution. The increase of methanol conversion and selectivity to
602 DME and light hydrocarbons could be finely controlled by increasing the zeolite
603 loading in the catalyst, for a given set reaction conditions.

604 Apparent kinetic parameters for the selective methanol dehydration to DME
605 were calculated assuming a reversible second order rate expression and
606 considering a plug flow integral reactor for the interpretation of the experimental
607 data. The calculated activation energy showed a value of 75 kJ/mol.

608 **Acknowledgements**

609 This work was supported by the Spanish Ministry of Sciences Innovation and
610 Universities and European Regional Development Fund (ERDF) through
611 RTI2018-097555-B-I00 project. J. Palomo acknowledges the assistance of the
612 Spanish Ministry of Education for the award of FPU grant (FPU13/02413). M. A.
613 Rodríguez-Cano also acknowledges the assistance of the Spanish Ministry of

Sciences Innovation and Universities for the concession of FPU grant (FPU18/02796).

References

[1] D.M. D'Alessandro, B. Smit, J.R. Long, Carbon Dioxide Capture: Prospects for New Materials, Angew. Chemie Int. Ed. 49 (2010) 6058–6082. https://doi.org/10.1002/anie.201000431.

[2] A. Corma, Inorganic Solid Acids and Their Use in Acid-Catalyzed Hydrocarbon Reactions, Chem. Rev. 95 (1995) 559–614. https://doi.org/10.1021/cr00035a006.

[3] D. Srinivasan, R. Rao, A. Zribi, Synthesis of novel micro- and mesoporous zeolite nanostructures using electrospinning techniques, J. Electron. Mater. 35 (2006) 504–509. https://doi.org/10.1007/BF02690538.

[4] A. Corma, From microporous to mesoporous molecular sieve materials and their use in catalysis, Chem. Rev. 97 (1997) 2373–2420. https://doi.org/10.1021/CR960406N.

[5] F. Pan, X. Lu, Q. Zhu, Z. Zhang, Y. Yan, T. Wang, S. Chen, A fast route for synthesizing nano-sized ZSM-5 aggregates, J. Mater. Chem. A. 2 (2014) 20667–20675. https://doi.org/10.1039/C4TA04073B.

[6] E. Catizzone, S. Van Daele, M. Bianco, A. Di Michele, A. Aloise, M. Migliori, V. Valtchev, G. Giordano, Catalytic application of ferrierite nanocrystals in vapour-phase dehydration of methanol to dimethyl ether, Appl. Catal. B Environ. 243 (2019) 273–282. https://doi.org/10.1016/j.apcatb.2018.10.060.

[7] S.F. Anis, A. Khalil, Saepurahman, G. Singaravel, R. Hashaikeh, A review on the fabrication of zeolite and mesoporous inorganic nanofibers formation for catalytic applications, Microporous Mesoporous Mater. 236 (2016) 176–192. https://doi.org/10.1016/J.MICROMESO.2016.08.043.

[8] F. Magzoub, X. Li, S. Lawson, F. Rezaei, A.A. Rownaghi, 3D-printed HZSM-5 and 3D-HZM5@SAPO-34 structured monoliths with controlled acidity and porosity for conversion of methanol to dimethyl either, Fuel. 280 (2020) 118628. https://doi.org/10.1016/J.FUEL.2020.118628.

[9] A. Trypolskyi, A. Zhokh, V. Gritsenko, M. Chen, J. Tang, P. Strizhak, A kinetic study on the methanol conversion to dimethyl ether over H-ZSM-5 zeolite, Chem. Pap. 2021 757. 75 (2021) 3429–3442. https://doi.org/10.1007/S11696-021-01586-Y.

[10] A. Aranzabal, D. Iturbe, M. Romero-Sáez, M.P. González-Marcos, J.R. González-Velasco, J.A. González-Marcos, Optimization of process parameters on the extrusion of honeycomb shaped monolith of H-ZSM-5 zeolite, Chem. Eng. J. 162 (2010) 415–423. https://doi.org/10.1016/J.CEJ.2010.05.043.

[11] Y. Park, Y. Ju, D. Park, C.-H. Lee, Adsorption equilibria and kinetics of six pure gases on pelletized zeolite 13X up to 1.0 MPa: CO2, CO, N2, CH4, Ar and H2, Chem. Eng. J. 292 (2016) 348–365. https://doi.org/10.1016/J.CEJ.2016.02.046.

[12] J. Pérez-Ramírez, C.H. Christensen, K. Egeblad, C.H. Christensen, J.C. Groen, Hierarchical zeolites: enhanced utilisation of microporous crystals in catalysis by advances in materials design, Chem. Soc. Rev. 37 (2008) 2530. https://doi.org/10.1039/b809030k.

[13] I. Yarulina, F. Kapteijn, J. Gascon, The importance of heat effects in the methanol to hydrocarbons reaction over ZSM-5: On the role of mesoporosity on catalyst performance, Catal. Sci. Technol. 6 (2016) 5320–5325. https://doi.org/10.1039/c6cy00654j.

[14] A.A. Rownaghi, F. Rezaei, M. Stante, J. Hedlund, Selective dehydration of methanol to dimethyl ether on ZSM-5 nanocrystals, Appl. Catal. B Environ. 119–120 (2012) 56–61. https://doi.org/10.1016/J.APCATB.2012.02.017.

[15] L. Treps, A. Gomez, T. De Bruin, C. Chizallet, Environment, Stability and Acidity of External Surface Sites of Silicalite-1 and ZSM-5 Micro and Nano Slabs, Sheets, and Crystals, ACS Catal. 10 (2020) 3297–3312. https://doi.org/10.1021/acscatal.9b05103.

[16] A. Palčić, E. Catizzone, Application of nanosized zeolites in methanol conversion processes: A short review, Curr. Opin. Green Sustain. Chem. 27 (2021) 1–8. https://doi.org/10.1016/j.cogsc.2020.100393.

[17] Svetlana Mintova, Maguy Jaber, Valentin Valtchev, Nanosized microporous crystals: emerging applications, Chem. Soc. Rev. 44 (2015) 7207–7233. https://doi.org/10.1039/C5CS00210A.

[18] E. Catizzone, S. Van Daele, M. Bianco, A. Di Michele, A. Aloise, M. Migliori, V. Valtchev, G. Giordano, Catalytic application of ferrierite nanocrystals in vapour-phase dehydration of methanol to dimethyl ether, Appl. Catal. B Environ. 243 (2019) 273–282. https://doi.org/10.1016/J.APCATB.2018.10.060.

[19] J. Park, J. Cho, M.J. Park, W.B. Lee, Microkinetic modeling of DME synthesis from methanol over H-zeolite catalyst: Associative vs.

688 dissociative pathways, Catal. Today. 375 (2021) 314–323.
689 https://doi.org/10.1016/J.CATTOD.2020.02.011.
690 [20] D. Li, B. Xing, B. Wang, R. Li, Activity and selectivity of methanol-to-olefin
691 conversion over Zr-modified H-SAPO-34/H-ZSM-5 zeolites - A theoretical
692 study, Fuel Process. Technol. 199 (2020) 106302.
693 https://doi.org/10.1016/J.FUPROC.2019.106302.
694 [21] D. Suttipat, K. Saenluang, W. Wannapakdee, P. Dugkhuntod, M.
695 Ketkaew, P. Pornsetmetakul, C. Wattanakit, Fine-tuning the surface
696 acidity of hierarchical zeolite composites for methanol-to-olefins (MTO)
697 reaction, Fuel. 286 (2021) 119306.
698 https://doi.org/10.1016/J.FUEL.2020.119306.
699 [22] T.A. Semelsberger, R.L. Borup, H.L. Greene, Dimethyl ether (DME) as an
700 alternative fuel, J. Power Sources. 156 (2006) 497–511.
701 https://doi.org/10.1016/j.jpowsour.2005.05.082.
702 [23] T.H. Fleisch, A. Basu, M.J. Gradassi, J.G. Masin, Dimethyl ether: A fuel
703 for the 21st century, Stud. Surf. Sci. Catal. 107 (1997) 117–125.
704 https://doi.org/10.1016/S0167-2991(97)80323-0.
705 [24] S.C. Sorenson, Dimethyl Ether in Diesel Engines : Progress and
706 Perspectives, J. Eng. Gas Turbines Power. 123 (2001) 652–658.
707 https://doi.org/10.1115/1.1370373.
708 [25] C. Arcoumanis, C. Bae, R. Crookes, E. Kinoshita, The potential of di-
709 methyl ether (DME) as an alternative fuel for compression-ignition
710 engines : A review, Fuel. 87 (2008) 1014–1030.
711 https://doi.org/10.1016/j.fuel.2007.06.007.
712 [26] Z. Azizi, M. Rezaeimanesh, T. Tohidian, M.R. Rahimpour, Dimethyl ether:

A review of technologies and production challenges, Chem. Eng. Process. Process Intensif. 82 (2014) 150–172. https://doi.org/10.1016/j.cep.2014.06.007.

[27] J. Sun, G. Yang, Y. Yoneyama, N. Tsubaki, Catalysis Chemistry of Dimethyl Ether Synthesis, ACS Catal. 4 (2014) 3346–3356. https://doi.org/10.1021/cs500967j.

[28] K. Saravanan, H. Ham, N. Tsubaki, J.W. Bae, Recent progress for direct synthesis of dimethyl ether from syngas on the heterogeneous bifunctional hybrid catalysts, Appl. Catal. B Environ. 217 (2017) 494–522. https://doi.org/10.1016/J.APCATB.2017.05.085.

[29] M. Rutkowska, D. Macina, Z. Piwowarska, M. Gajewska, U. Díaz, L. Chmielarz, Hierarchically structured ZSM-5 obtained by optimized mesotemplate-free method as active catalyst for methanol to DME conversion, Catal. Sci. Technol. 6 (2016) 4849–4862. https://doi.org/10.1039/c6cy00040a.

[30] C. Mei, P. Wen, Z. Liu, H. Liu, Y. Wang, W. Yang, Z. Xie, W. Hua, Z. Gao, Selective production of propylene from methanol: Mesoporosity development in high silica HZSM-5, J. Catal. 258 (2008) 243–249. https://doi.org/10.1016/J.JCAT.2008.06.019.

[31] D. Prinz, L. Riekert, Formation of ethene and propene from methanol on zeolite ZSM-5: I. Investigation of Rate and Selectivity in a Batch Reactor, Appl. Catal. 37 (1988) 139–154. https://doi.org/10.1016/S0166-9834(00)80757-5.

[32] S. Ivanova, E. Vanhaecke, L. Dreibine, B. Louis, C. Pham, C. Pham-Huu, Binderless HZSM-5 coating on β-SiC for different alcohols dehydration,

738 Appl. Catal. A Gen. 359 (2009) 151–157.
739 https://doi.org/10.1016/J.APCATA.2009.02.024.
740 [33] Y. Zhang, Q. Wang, B. Louis, ZSM-5 zeolite coatings on perlite support
741 for MTO application, Microporous Mesoporous Mater. 323 (2021) 111172.
742 https://doi.org/10.1016/J.MICROMESO.2021.111172.
743 [34] R. Ruiz-Rosas, J. Bedia, J.M. Rosas, M. Lallave, I.G. Loscertales, J.
744 Rodríguez-Mirasol, T. Cordero, Methanol decomposition on electrospun
745 zirconia nanofibers, Catal. Today. 187 (2012) 77–87.
746 https://doi.org/10.1016/j.cattod.2011.10.031.
747 [35] F.J. García-Mateos, R. Berenguer, M.J. Valero-Romero, J. Rodríguez-
748 Mirasol, T. Cordero, Phosphorus functionalization for the rapid
749 preparation of highly nanoporous submicron-diameter carbon fibers by
750 electrospinning of lignin solutions, J. Mater. Chem. A. 6 (2018) 1219–
751 1233. https://doi.org/10.1039/C7TA08788H.
752 [36] I.G. Loscertales, A. Barrero, M. Márquez, R. Spretz, R. Velarde-Ortiz, G.
753 Larsen, Electrically Forced Coaxial Nanojets for One-Step Hollow
754 Nanofiber Design, J. Am. Chem. Soc. 126 (2004) 5376–5377.
755 https://doi.org/10.1021/JA049443J.
756 [37] J. Liu, G. Jiang, Y. Liu, J. Di, Y. Wang, Z. Zhao, Q. Sun, C. Xu, J. Gao, A.
757 Duan, J. Liu, Y. Wei, Y. Zhao, L. Jiang, Hierarchical Macro-meso-
758 microporous ZSM-5 Zeolite Hollow Fibers With Highly Efficient Catalytic
759 Cracking Capability, Sci. Rep. 4 (2015) 7276.
760 https://doi.org/10.1038/srep07276.
761 [38] J. Palomo, M.Á. Rodríguez-Cano, J. Rodríguez-Mirasol, T. Cordero,
762 ZSM-5-decorated CuO/ZnO/ZrO2 fibers as efficient bifunctional catalysts

763 for the direct synthesis of DME from syngas, Appl. Catal. B Environ. 270
764 (2020) 118893. https://doi.org/10.1016/j.apcatb.2020.118893.
765 [39] S.F. Anis, R. Hashaikeh, Electrospun zeolite-Y fibers: Fabrication and
766 morphology analysis, Microporous Mesoporous Mater. 233 (2016) 78–86.
767 https://doi.org/10.1016/J.MICROMESO.2015.11.022.
768 [40] K.S. Ha, Y.J. Lee, J.W. Bae, Y.W. Kim, M.H. Woo, H.S. Kim, M.J. Park,
769 K.W. Jun, New reaction pathways and kinetic parameter estimation for
770 methanol dehydration over modified ZSM-5 catalysts, Appl. Catal. A Gen.
771 395 (2011) 95–106. https://doi.org/10.1016/j.apcata.2011.01.025.
772 [41] S. Brunauer, P.H. Emmett, E. Teller, Adsorption of Gases in
773 Multimolecular Layers, J. Am. Chem. Soc. 60 (1938) 309–319.
774 https://doi.org/10.1021/ja01269a023.
775 [42] S. Lowell, J.E. Shields, J.E. Morral, Powder Surface Area and Porosity,
776 2nd Edition, 1985. https://doi.org/10.1115/1.3225796.
777 [43] M.M. Dubinin, The Potential Theory of Adsorption of Gases and Vapors
778 for Adsorbents with Energetically Nonuniform Surfaces., Chem. Rev. 60
779 (1960) 235–241. https://doi.org/10.1021/cr60204a006.
780 [44] G.K. Williamson, W.H. Hall, X-ray line broadening from filed aluminium
781 and wolfram, Acta Metall. 1 (1953) 22–31. https://doi.org/10.1016/0001-
782 6160(53)90006-6.
783 [45] Y. Jin, D. Yang, D. Kang, X. Jiang, Fabrication of Necklace-like Structures
784 via Electrospinning, Langmuir. 26 (2010) 1186–1190.
785 https://doi.org/10.1021/la902313t.
786 [46] S. Jiang, W. He, K. Landfester, D. Crespy, S.E. Mylon, The structure of
787 fibers produced by colloid-electrospinning depends on the aggregation

state of particles in the electrospinning feed, Polymer (Guildf). 127 (2017) 101–105. https://doi.org/10.1016/J.POLYMER.2017.08.061.

[47] M. Thommes, K. Kaneko, A. V. Neimark, J.P. Olivier, F. Rodriguez-Reinoso, J. Rouquerol, K.S.W. Sing, Physisorption of gases, with special reference to the evaluation of surface area and pore size distribution (IUPAC Technical Report), Pure Appl. Chem. 87 (2015). https://doi.org/10.1515/pac-2014-1117.

[48] J.C. Groen, L.A.A. Peffer, J.A. Moulijn, J. Pérez-Ramírez, Mechanism of Hierarchical Porosity Development in MFI Zeolites by Desilication: The Role of Aluminium as a Pore-Directing Agent, Chem. - A Eur. J. 11 (2005) 4983–4994. https://doi.org/10.1002/chem.200500045.

[49] J. Pérez-Ramírez, R.J. Berger, G. Mul, F. Kapteijn, J.A. Moulijn, The six-flow reactor technology: A review on fast catalyst screening and kinetic studies, Catal. Today. 60 (2000) 93–109. https://doi.org/10.1016/S0920-5861(00)00321-7.

[50] D.E. Mears, The role of axial dispersion in trickle-flow laboratory reactors, Chem. Eng. Sci. 26 (1971) 1361–1366. https://doi.org/10.1016/0009-2509(71)80056-8.

[51] J.A. Moulijn, A. Tarfaoui, F. Kapteijn, General aspects of catalyst testing, Catal. Today. 11 (1991) 1–12. https://doi.org/10.1016/0920-5861(91)87002-5.

[52] O. Levenspiel, Engineering Flow and Heat Exchange, Springer US, Boston, MA, 2014. https://doi.org/10.1007/978-1-4899-7454-9.

[53] G.W. Jackson, D.F. James, The permeability of fibrous porous media, Can. J. Chem. Eng. 64 (1986) 364–374.

https://doi.org/10.1002/cjce.5450640302.

[54] E. Mauret, M. Renaud, Transport phenomena in multi-particle systems—I. Limits of applicability of capillary model in high voidage beds-application to fixed beds of fibers and fluidized beds of spheres, Chem. Eng. Sci. 52 (1997) 1807–1817. https://doi.org/10.1016/S0009-2509(96)00499-X.

[55] J. Palomo, M.A. Rodríguez-Cano, J. Rodríguez-Mirasol, T. Cordero, On the kinetics of methanol dehydration to dimethyl ether on Zr-loaded P-containing mesoporous activated carbon catalyst, Chem. Eng. J. 378 (2019). https://doi.org/10.1016/j.cej.2019.122198.

[56] J.C. Bedoya, R. Valdez, L. Cota, M.A. Alvarez-Amparán, A. Olivas, Performance of Al-MCM-41 nanospheres as catalysts for dimethyl ether production, Catal. Today. (2021) 1–8. https://doi.org/10.1016/j.cattod.2021.01.010.

[57] M.A. Armenta, V.M. Maytorena, L.A. Flores–Sánchez, J.M. Quintana, R. Valdez, A. Olivas, Dimethyl ether production via methanol dehydration using Fe3O4 and CuO over γ–χ–Al2O3 nanocatalysts, Fuel. 280 (2020) 118545. https://doi.org/10.1016/j.fuel.2020.118545.

[58] M.A. Armenta, V.M. Maytorena, R. Silva-Rodrigo, L.A. Flores-Sánchez, J.M. Quintana, A. Olivas, Effect of acidity on ferric oxide nanoparticles supported on γ–χ–Al2O3 in the methanol dehydration reaction toward dimethyl ether, Fuel. 296 (2021). https://doi.org/10.1016/j.fuel.2021.120618.

[59] Y.H. Seo, E.A. Prasetyanto, N. Jiang, S.M. Oh, S.E. Park, Catalytic dehydration of methanol over synthetic zeolite W, Microporous Mesoporous Mater. 128 (2010) 108–114.

https://doi.org/10.1016/j.micromeso.2009.08.011.

[60] E. Catizzone, A. Aloise, E. Giglio, G. Ferrarelli, M. Bianco, M. Migliori, G. Giordano, MFI vs. FER zeolite during methanol dehydration to dimethyl ether: The crystal size plays a key role, Catal. Commun. 149 (2021) 106214. https://doi.org/10.1016/J.CATCOM.2020.106214.

[61] B.T. Diep, M.S. Wainwright, Thermodynamic Equilibrium Constants for the Methanol-Dimethyl Ether-Water System, J. Chem. Eng. Data. 32 (1987) 330–333. https://doi.org/10.1021/JE00049A015.

[62] S.J. Royaee, C. Falamaki, M. Sohrabi, S.S. Ashraf Talesh, A new Langmuir-Hinshelwood mechanism for the methanol to dimethylether dehydration reaction over clinoptilolite-zeolite catalyst, Appl. Catal. A Gen. 338 (2008) 114–120. https://doi.org/10.1016/j.apcata.2008.01.011.

[63] Y. Tavan, S.H. Hosseini, From laboratory experiments to simulation studies of methanol dehydration to produce dimethyl ether reaction-Part II: Simulation and cost estimation, Chem. Eng. Process. 73 (2013) 144–150. https://doi.org/10.1016/j.cep.2013.08.006.

[64] Y. Tavan, R. Hasanvandian, Two practical equations for methanol dehydration reaction over HZSM-5 catalyst - Part I: Second order rate equation, Fuel. 142 (2015) 208–214. https://doi.org/10.1016/j.fuel.2014.10.078.

[65] C. Ortega, M. Rezaei, V. Hessel, G. Kolb, Methanol to dimethyl ether conversion over a ZSM-5 catalyst: Intrinsic kinetic study on an external recycle reactor, Chem. Eng. J. 347 (2018) 741–753. https://doi.org/10.1016/J.CEJ.2018.04.160.

[66] W. Alharbi, E.F. Kozhevnikova, I. V. Kozhevnikov, Dehydration of

Methanol to Dimethyl Ether over Heteropoly Acid Catalysts: The Relationship between Reaction Rate and Catalyst Acid Strength, ACS Catal. 5 (2015) 7186–7193. https://doi.org/10.1021/acscatal.5b01911.

[67] P. Pérez-Uriarte, A. Ateka, A.T. Aguayo, A.G. Gayubo, J. Bilbao, Kinetic model for the reaction of DME to olefins over a HZSM-5 zeolite catalyst, Chem. Eng. J. 302 (2016) 801–810. https://doi.org/10.1016/J.CEJ.2016.05.096.

[68] T. Cordero-Lanzac, A. Ateka, P. Pérez-Uriarte, P. Castaño, A.T. Aguayo, J. Bilbao, Insight into the Deactivation and Regeneration of HZSM-5 Zeolite Catalysts in the Conversion of Dimethyl Ether to Olefins, Ind. Eng. Chem. Res. 57 (2018) 13689–13702. https://doi.org/10.1021/ACS.IECR.8B03308.

[69] B. Louis, F. Ocampo, H.S. Yun, J.P. Tessonnier, M.M. Pereira, Hierarchical pore ZSM-5 zeolite structures: From micro- to macro-engineering of structured catalysts, Chem. Eng. J. 161 (2010) 397–402. https://doi.org/10.1016/J.CEJ.2009.09.041.

[70] S. Ivanova, B. Louis, B. Madani, J. P. Tessonnier, A. M. J. Ledoux, C. Pham-Huu, ZSM-5 Coatings on β-SiC Monoliths: Possible New Structured Catalyst for the Methanol-to-Olefins Process, J. Phys. Chem. C. 111 (2007) 4368–4374. https://doi.org/10.1021/JP067535K.

[71] P. Tian, Y. Wei, M. Ye, Z. Liu, Methanol to olefins (MTO): From fundamentals to commercialization, ACS Catal. 5 (2015) 1922–1938. https://doi.org/10.1021/acscatal.5b00007.

[72] D. Rojo-Gama, M. Signorile, F. Bonino, S. Bordiga, U. Olsbye, K.P. Lillerud, P. Beato, S. Svelle, Structure–deactivation relationships in

zeolites during the methanol–to-hydrocarbons reaction: Complementary assessments of the coke content, J. Catal. 351 (2017) 33–48. https://doi.org/10.1016/j.jcat.2017.04.015.

[73] M. Ibáñez, P. Pérez-Uriarte, M. Sánchez-Contador, T. Cordero-Lanzac, A.T. Aguayo, J. Bilbao, P. Castaño, Nature and Location of Carbonaceous Species in a Composite HZSM-5 Zeolite Catalyst during the Conversion of Dimethyl Ether into Light Olefins, Catal. 2017, Vol. 7, Page 254. 7 (2017) 254. https://doi.org/10.3390/CATAL7090254.